Article

Journal of
Nanoscience and Nanotechnology
Vol. 18, 1–9, 2018
www.aspbs.com/jnn

Characterization and Photocatalytic Performance of Potassium-Doped Titanium Oxide Nanostructures Prepared via Wet Corrosion of Titanium Microspheres

So Yoon Lee[1], Jie Zhang[1], Lee-Woon Jang[1], Zhihong Zhang[1], Yujie Guo[1], Samir Salameh[2], Sanghoon Kim[3], Dong Ick Son[4], Vijay Shankar Rangasamy[5], Savitha Thayumanasundaram[5], Jean-Pierre Locquet[5], and Jin Won Seo[1,*]

[1] *Department of Materials Engineering, KU Leuven, B-3001 Leuven, Belgium*
[2] *Institut für Werkstofftechnik, Universität Bremen, D-28359 Bremen, Germany*
[3] *Department of Materials Science and Engineering, Yonsei University, Seoul 120-749, Republic of Korea*
[4] *Soft Innovative Materials Research Center, Korea Institute of Science and Technology, Wanju, 565-90, Republic of Korea*
[5] *Department of Physics, KU Leuven, B-3001 Leuven, Belgium*

Potassium doped titanium oxide ($KTiO_x$) nanowires were prepared by the wet corrosion process (WCP) and their photocatalytic effects were systematically characterized. For the synthesis of $KTiO_x$, the potassium hydroxide concentration of the WCP was varied in order to obtain nanostructures with different surface area and surface charge. Structural and crystalline properties of $KTiO_x$ were studied by means of X-ray diffraction, scanning and transmission electron microscopy. Chemical composition was determined by X-ray fluorescence and energy-dispersive X-ray analysis. Photocatalytic performance was investigated as a function of the surface area, pH, and crystalline structures by studying the degradation of methylene blue, cardiogreen, and azorubine red dyes upon UV irradiation. The negatively charged crystalline $KTiO_x$ nanostructures with high surface area showed significantly higher photocatalytic degradation compared to their TiO_x counterpart. They also showed high efficiency for recovery and re-use. Annealing $KTiO_x$ nanostructures improved structural properties leading to well-ordered layered structures and improved photocatalysis. However, annealing at temperatures higher than 600 °C yielded formation of rutile grains at the surface of nanowires, significantly affecting the photocatalytic performance. We believe that $KTiO_x$ nanostructures produced by WCP are very promising for photocatalysis, especially due to their high photocatalytic efficiency as well as their potential for re-use and durability.

Keywords: $KTiO_x$, Titanium Core Shell, Nanostructures, Photocatalysis, Wet Corrosion Process.

1. INTRODUCTION

Titanium (Ti)-based materials have widely been studied because of its abundance, low cost, excellent chemical stability, environmental benignity, high photocatalytic activity and antimicrobial properties. Especially, titanium oxide (TiO_x) materials have attracted considerable interests in many fields of research including photovoltaics and photocatalysis.[1–6] Generally, when TiO_2 is exposed to adequate photon energy of <400 nm, electron–hole pairs are generated on the surface.[7–9] For the photocatalytic application, these electron–hole pairs react with target molecules and degrade them. Commonly, monodispersed TiO_2 nanoparticles and nanowires have extensively been studied because of their large surface area[10–13] and strong light absorption.[14–16] In addition, the photocatalytic efficiency could be enhanced by controlling adsorption–desorption process via surface charges by changing pH or by applying alkaline doping.[17–19] In particular, for K-doped $KTiO_x$, the K doping promoted the stabilization of the anatase phase and also yielded higher efficacy of photocatalytic activity.[20–22] Recently, the wet corrosion process (WCP) was applied to Ti metal substrates and a network of $KTiO_x$ nanowires could be obtained on the metal

*Author to whom correspondence should be addressed.

surface.[19, 23, 24] The WCP relies on potassium hydroxide (KOH) treatment of Ti metal and has demonstrated high efficiency and high reproducibility in producing nanostructured surface with a high surface area and with varying potassium doping. The produced $KTiO_x$ nanostructures showed high photocatalytic performances[19, 25] and could also successfully be used in dye-sensitized solar cells.[26]

The WCP is a simple one-step synthesis method at room-temperature without any supplementary treatments.[19, 23, 24, 27] The formation of $KTiO_x$ nanowires is directly affected by the solution concentration,[19] which also changes the K content in the nanostructures formed on the surface. Simultaneously, the surface area as well as the photocatalytic activity scales with the KOH concentration. Thus, the WCP is a promising method for the efficient and well-tunable production of $KTiO_x$ nanostructures. So far, the basic principle of WCP was studied and a few applications of $KTiO_x$ nanostructures have been reported, while a more detailed characterization is missing.

In this work, we synthesized $KTiO_x$ nanowires on Ti microspheres by the WCP. The influence of the surface area and the effect of the surface charge were investigated. Structural and chemical evolution of $KTiO_x$ were studied as a function of the annealing temperature. Additionally, the photocatalytic performance was derived from degradation of three organic dyes: methylene blue (MB), cardiogreen (CG) and azorubine red (AR), which represent potential pollutants in colored waste water. The negatively charged $KTiO_x$ annealed at 600 °C showed the highest catalytic activity in all three tested dyes. These nanostructures are also highly suitable for recycling and re-use, especially for MB dyes a high recovery performance of about 97% was measured.

2. EXPERIMENTAL DETAILS

Ti microspheres (purity >99.8%, diameter of 125–250 μm) were purchased from ChemPUR in Germany.[19] Ti particles were soaked in 5 mL KOH solution with concentration of 1, 5, 10, 15, 20, and 25 mol/L at room temperature for 24 hours. After this WCP step of the KOH treatment, all particles were washed with deionized water and dried. These particles contained a Ti core and a shell of $KTiO_x$ nanowire forming a network. Subsequently, the particles were annealed at 300, 450, 600 and 750 °C for 2 hours in an oxygen-rich furnace (Carbolite GSM furnace 3216) to study their crystalline structure as a function of the annealing temperature.

Scanning electron microscope (SEM) combined with a focused ion beam (FIB, Dual Beam FEI Nova 600 NanoLab) was used to measure the surface structure, shape and size of $KTiO_x$. For identification and visualization of the $KTiO_x$ shell and Ti core structure, the WCP treated particles were sliced by FIB with 30 kV Ga-ions, and cross-sectional parts were analyzed by energy-dispersive X-ray (EDX, EDAX) spectroscopy. X-ray fluorescence (XRF, Philips PW2400, source: 50 kV, 40 mA) was measured for the quantitative elemental analysis. Transmission electron microscopy (TEM) and scanning transmission electron microscopy (STEM) were carried out using a probe-lens aberration-corrected microscope ARM200F (JEOL) equipped with a cold-field emission gun and the large-angle EDX spectrometer (Centurio, JEOL). For these measurements, a few spheres were glued directly on a half Cu grid (100 mesh, Agar Scientific).

Surface area analysis was performed by using NOVA 300E (Quantachrome), which estimates the surface area by nitrogen adsorption behaviors. The surface area was calculated based on the Brunauer-Emmett and Teller (BET) theory. Zeta potentials were measured by using an electrophoretic light scattering spectrophotometer in order to analyze the surface charge of the $KTiO_x$ shell after treating at various conditions of pH. A quartz cell was used to measure the electrophoretic mobility of polystylene latex reference particles. The pH value was adjusted using aqueous solution of NaOH and HCl.

In order to evaluate the photocatalytic activity of the $KTiO_x$, 0.1 g of particles was taken and mixed with 2 ml of MB (10 mg/L), CG (10 mg/L) and AR (10 mg/L) dye solutions separately under UV irradiation (320∼390 nm, 159×229 mm lamp) with 10 cm working distance. During the UV exposure, the solutions were stirred continuously. However, experiments performed without stirring didn't show any significant difference. After UV irradiation, the photocatalytic activity was evaluated by collecting the UV-Vis absorption spectra (Tecan, Model infinite M2000 PRO) of the solution. The recycle and re-use potential of $KTiO_x$ nanostructures were evaluated by collecting a series of repeated photocatalytic reaction experiments under the same condition as described above. Deionized water, ethanol and iso-propanol were used for rinsing the $KTiO_x$ after each treatment. The degradation efficiency was recorded after each cycle.

3. RESULTS AND DISCUSSION

3.1. Morphology of the Synthesized $KTiO_x$

The resulting surface morphology strongly depended on the concentration of the treating KOH solution. Representative surface images of pristine Ti particles and KOH treated Ti particles are shown in Figure 1. The 1 mol/L and 15 mol/L KOH treated Ti particles showed the smallest and the largest surface areas, respectively. For concentrations below 20 mol/L, elongated nanowires with diameter of 10∼100 nm and length of several tens of micrometers were observed. This result is very comparable with our previous results obtained on Ti plates.[19] Thus, WCP enables nanostructures fabrication starting from various Ti-containing materials regardless of the shape of the material. In the cross-sectional image of Figure 1(d), the Ti core

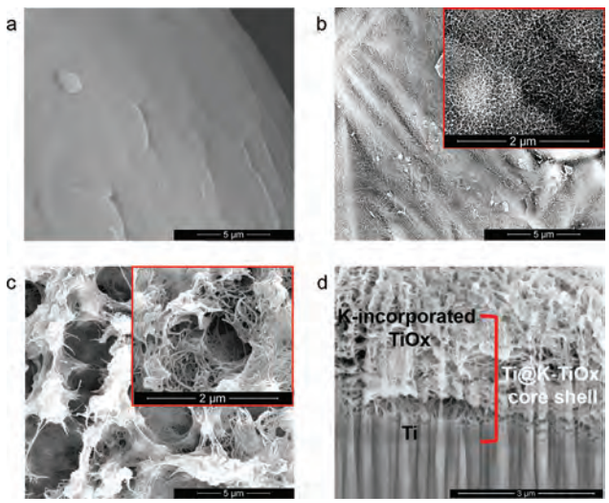

Figure 1. SEM images of (a) a Ti particle, (b) a 1 mol/L KOH treated Ti particle, and (c) a 15 mol/L KOH treated Ti particle at RT for 24 hours. The respective insets present enlarged images of the surface structures. (d) The cross-section image of a 15 mol/L KOH treated Ti particle reveals the interface area between the $KTiO_x$ shell and the Ti core. The vertical striations originate from the FIB etching due to the curtaining effect.

and porous $KTiO_x$ shell can clearly be seen. The total shell thickness was approximately 5 μm.

3.2. Chemical Analysis of the $KTiO_x$ Nanostructures

EDX measurements performed on the cross-sectioned interface between the Ti core and the $KTiO_x$ shell clearly confirmed the K doping (Fig. 2). The shell area (Fig. 2(a)) with the nanowire networks resulted in clear EDX peaks of K (3.31 keV and 0.26 keV) and O (0.52 keV) whereas these peaks significantly decreased when moving the electron beam towards the Ti core (Fig. 2(b)), and completely disappeared in the core area. The color-coded EDX map presented in the inset of Figure 2(a) illustrates that the interface is not abrupt and that a transition area exists in the range of several micrometers. Figure 2(c) shows a TEM image of the $KTiO_x$ nanowires with a diameter in the range of 10–30 nm. The presence of K in the individual $KTiO_x$ nanowires was confirmed by STEM-based EDX mapping. Quantitative analysis yielded a K-concentration of about 4.5 ± 1.1 wt%.

Figure 3 shows the result of XRF measurements for the KOH treated Ti particles as a function of the K content. With increasing KOH concentration from 0 to 15 mol/L, the incorporated amount of K increased linearly, whereas above the critical concentration (>15 mol/L), the slope slightly flattens indicating that the incorporation of K in $KTiO_x$ surface structure reaches a first saturation point and further incorporation of K becomes more difficult during the WCP. The K content measured in the sample of 15 mol/L KOH treated Ti was about 4.4 ± 0.1 wt%, which is in agreement with the STEM-EDX result of 4.5 ± 1.1 wt%.

3.3. Analysis of the Surface Area of $KTiO_x$ Nanostructures

BET analysis was performed in order to measure the increase of the surface area. The surface area profile is presented in Figure 4 as a function of concentration of the KOH solutions. The surface area gradually increased with the KOH concentration in agreement with the SEM results (Fig. 1), where the structural evolution from individual thick and short nanostructures to three-dimensional network of thin and elongated nanowires was observed. Accordingly, we can conclude that the WCP induced strong morphology changes with the KOH concentration. These changes effectively go together with an enlargement of the surface area.

3.4. Analysis of Surface Charge of $KTiO_x$ Nanostructures

Figure 5 shows the zeta potential measured for the 15 mol/L KOH treated Ti particles in various pH levels. For TiO_2 particles, previous studies reported that the isoelectric point (IEP) ranged from 5.1 to 6.7, and the surface potential was rather positive.[28–31] In contrast, the surface potential of the $KTiO_x$ is negative and the IEP for 15 mol/L KOH treated Ti particles is about 4.0. This is attributed to the formation of OH groups on the surface during the WCP. These OH groups can be a source of the negative charge observed and influence the electronegativity of the materials ions.[32, 33] It has to be noted that the $KTiO_x$ nanowires show a large pH region of negatively charged surface, which is a valuable characteristic to conjugate the organic dyes without additional treatments.

3.5. Analysis of the Crystalline Structure of $KTiO_x$

For TiO_2, the anatase phase is known to be more photocatalytically active compared with the rutile phase.[34] Especially for nanoscale TiO_x, the formation of the anatase phase seems to be promoted due to the lower surface free energy.[35] The transition from anatase to rutile phase is within the range of 400–1200 °C.[36] In order to study the effect of crystalline structure, the samples were annealed at temperatures between 300 to 750 °C. The annealing didn't lead to any significant change in the particles size or shape. Also in terms of dispersion, the annealed particles didn't show any difference. Figure 6(a) shows surface morphologies of $KTiO_x$ nanowires after annealing at different temperatures observed by SEM. As can be seen, the annealing has no significant effect below 600 °C, and $KTiO_x$ nanostructures showed similar diameters of about 30 nm. In contrast, the nanowires annealed at 750 °C yielded much larger diameter of approximately 100 nm. Figure 6(b) shows XRD spectra obtained from the Ti spheres containing $KTiO_x$ nanowires annealed at different temperatures. For all spectra, the most predominant peaks originate from the Ti core. The peaks corresponding to $KTiO_x$ are hardly visible in the WCP material as well

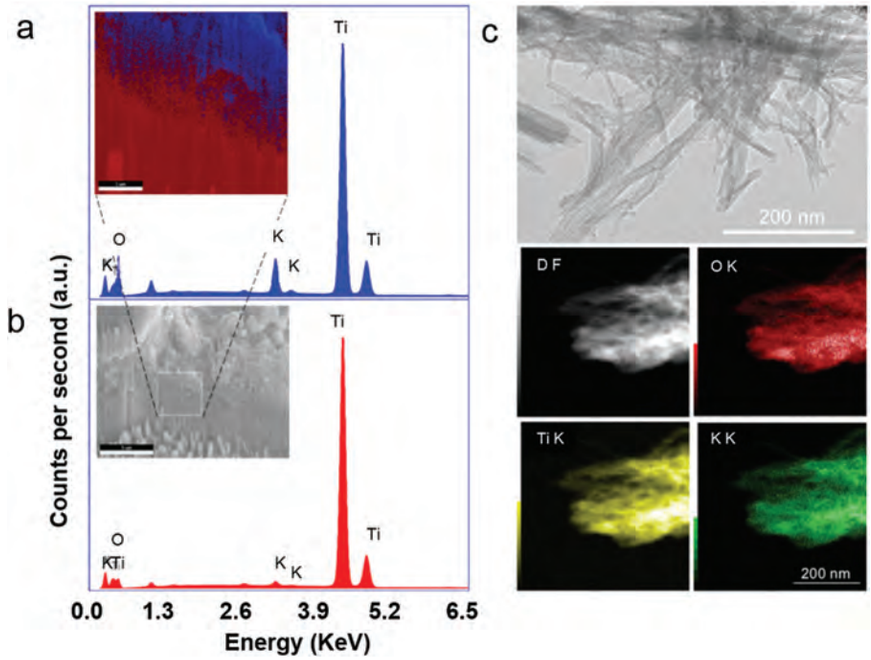

Figure 2. SEM-EDX spectra taken from the cross-sectional interface between (a) the $KTiO_x$ shell and (b) the Ti core. The corresponding SEM image can be seen in the inset of (b) whereas the inset of (a) shows the EDX map of the interface area marked by white rectangle in the SEM image. The color-code matches with the color of the EDX spectra: K-rich and K-poor areas are colored blue and red, respectively. (c) TEM image of $KTiO_x$ nanowires present in the outer shell-area of the Ti particle. The dark-field STEM image (DF) and the EDX-maps (O-, K- and Ti-maps) taken from the nanowires evidence the presence of $KTiO_x$.

as in the samples annealed below 600 °C. For the sample annealed at 600 °C small peaks appear. Finally after annealing at 750 °C, peaks corresponding to the anatase and the rutile phases can clearly be identified, as indicated in Figure 6(b). In a detailed analysis, the peaks observed at 27.8°, 41.75° and 48.24° could be correlated with (110) and (111) peaks of the rutile phase and (200) peak of the anatase phase, respectively.

$KTiO_x$ nanowires annealed at different temperatures were investigated by high-resolution TEM. In Figure 7, those annealed at 600 °C and 750 °C are presented. As can be seen in Figure 7(b), the nanowires annealed at 600 °C contain well-crystallized structure with lattice fringes appearing parallel with the nanowire axis. The spacing of the fringes was about 0.85 nm as also confirmed by the Fast-Fourier-Transform (FFT) pattern in Figure 7(c). Perpendicular to the nanowire axis, a lattice spacing of 0.36 nm was measured, which is in agreement with $d_{(101)}$ of the TiO_2 anatase phase. The large d spacing

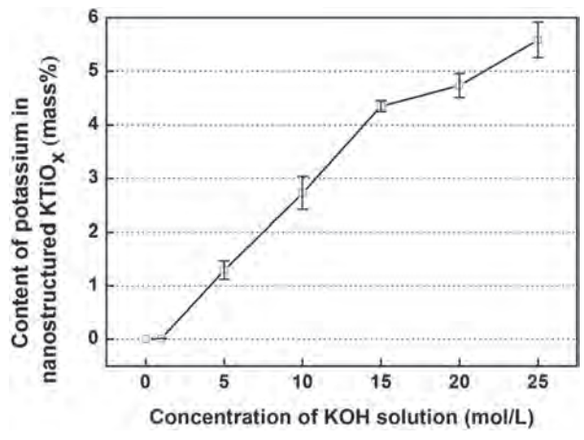

Figure 3. XRF measurements revealing the potassium content in the nanostructured $KTiO_x$ obtained after KOH treatments of Ti particles with different concentrations.

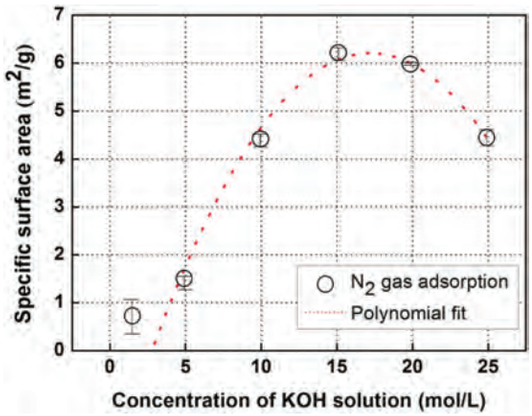

Figure 4. Surface areas of KOH treated Ti particles derived from BET analysis. By increasing KOH concentration, the surface area of $KTiO_x$ increased. A maximum surface area was achieved at 15 mol/L with a specific surface area of about 6.1 m^2/g.

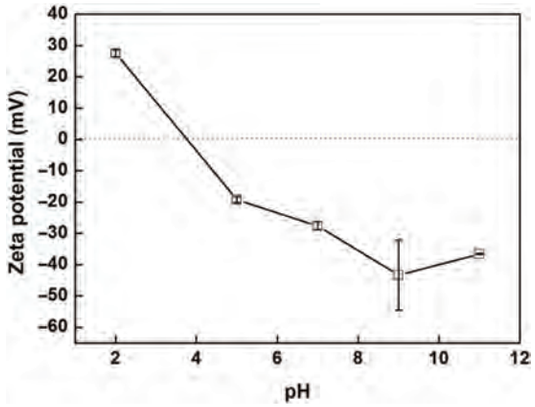

Figure 5. Zeta potential measured for the 15 mol/L KOH treated Ti particles as a function of pH.

of about 0.85 nm does not correspond to any plane in the anatase or rutile crystal structures. However, potassium titanates are well known to form a layered or tunnel structure by zig-zag layers of titanium-oxygen octahedra separated by K_2O.[37] The obtained value is close to that previously reported for $K_{0.06}TiO_2$ (0.72 nm)[38] or $K_2Ti_8O_{17}$ (0.78 nm).[39]

For samples annealed at lower temperatures, similar high-resolution TEM images were obtained but the lattice fringes were less well pronounced indicating that the crystallinity improved with the annealing temperature. However, annealing at 750 °C leads to the formation of crystallites with a diameter of a few nm on the nanowire surface. In the core-region, the wide-spaced lattice fringes remain. In the FFT pattern (Fig. 7(f)), a series of diffraction spots arranged in concentric rings can be seen. They could be matched with $d_{(111)}$ and $d_{(211)}$ of the rutile phase. EDX analysis revealed a slightly reduced K-concentration. The structural transformation from the layered structure to rutile structure may be promoted by the loss of K atoms.

3.6. Photocatalytic Activity of the $KTiO_x$ Nanostructures

3.6.1. Effect of the Surface Area

Generally, the photocatalytic activity leading to degradation of dyes depends on the catalyst concentration. The high surface area exerts a synergistic effect on catalyst concentration. Since the higher catalyst concentration induces an increase of the adsorbed dye molecules, higher photocatalytic performance can be expected.[30] In order to evaluate the photocatalytic activity, we monitored the degradation of MB dyes upon UV irradiation. Figure 8(a) shows the effect of the WCP on photocatalytic degradation of MB. The Ti particles treated with 15 mol/L KOH solution, which has the highest surface area (see Fig. 4), yielded significantly higher photocatalytic efficiency. The UV-Vis absorption results shown in Figure 8(b) clearly confirm this trend: The characteristic absorption intensity of MB dye at 664 nm decreased under UV irradiation, indicating the dye degradation. The 15 mol/L KOH treated Ti particles showed remarkable photocatalytic degradation of MB dye with approximately 90% degradation upon 2 hours of UV light exposure, compared to 50% and 40% degradation for the 1 mol/L KOH treated Ti particles and raw Ti particles, respectively. Taking the BET analysis (see Fig. 3) into account, where the surface area of 15 mol/L KOH treated Ti particles was about 8 times higher than that of the 1 mol/L KOH treated Ti particles, it can be concluded that the enhanced photocatalytic activity directly

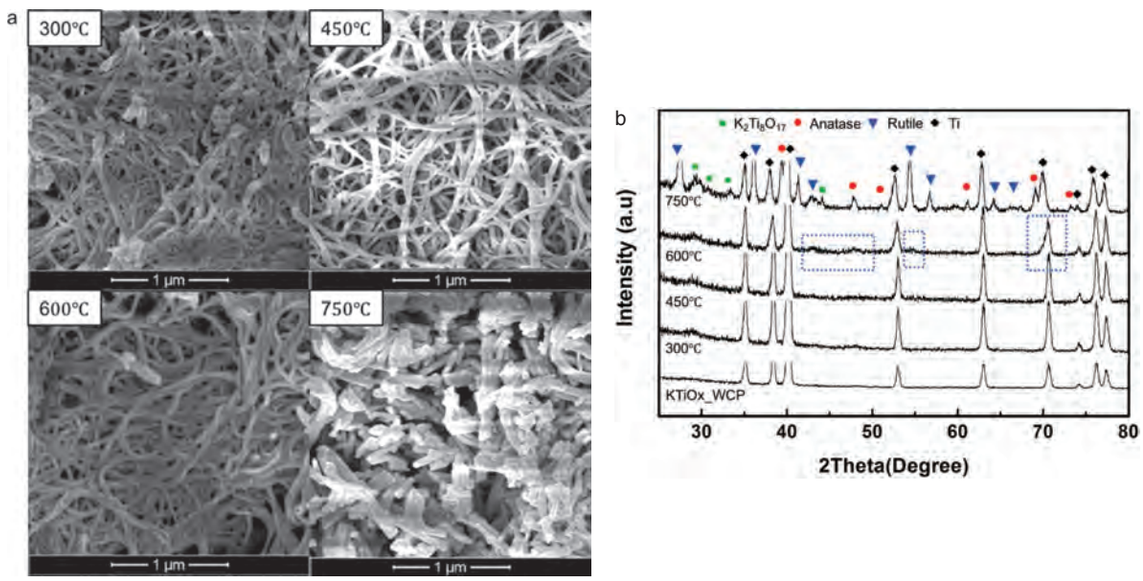

Figure 6. (a) SEM images of $KTiO_x$ annealed at 300, 450, 600 and 750 °C; (b) XRD spectra of $KTiO_x$/Ti microspheres annealed at different temperatures. The peaks corresponding to the anatase and the rutile phases are marked with spheres and triangles.

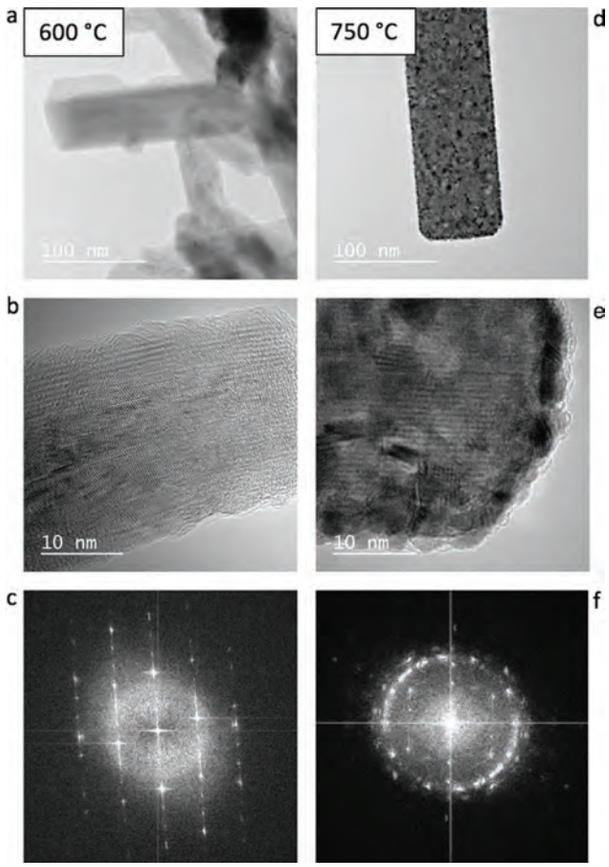

Figure 7. (a, b) TEM images of $KTiO_x$ annealed at 600 °C show that the nanowires are crystalline with well-defined layered structure with a spacing of about 0.8 nm. (d, e) TEM images of $KTiO_x$ annealed at 750 °C reveal crystallites of a few nanometer in size, which give the nanowire speckled contrast. The respective FFT patterns (c and f) confirm the crystalline structure. The diffraction spots arranged in concentric rings in (f) can be matched with lattice spacings of the TiO_2 rutile structure.

correlates with the increased surface area, in agreement with previous reports.[6, 40] This photodegradation efficiency of the produced $KTiO_x$ can also be determined quantitatively based on the evolution of the peak height at 664 nm, using the pseudo-first order model as follows:[41]

$$\ln(C_0/C_t) = kt$$

where C_0 and C_t are the concentrations of dye at the time $t = 0$ and time t, respectively, and k is the pseudo-first order rate constant. As presented in Table I, the 15 mol/L KOH Ti particles with the highest surface area revealed a C/C_0 ratio of 0.09, which is significantly lower than that of the untreated sample with 0.87, indicating the high degree of degradation. Also compared with pure TiO_2 particles of the same size, the C/C_0 ratio is about eight times smaller. This result clearly confirms the role of the high surface area leading to high photocatalytic efficiency.

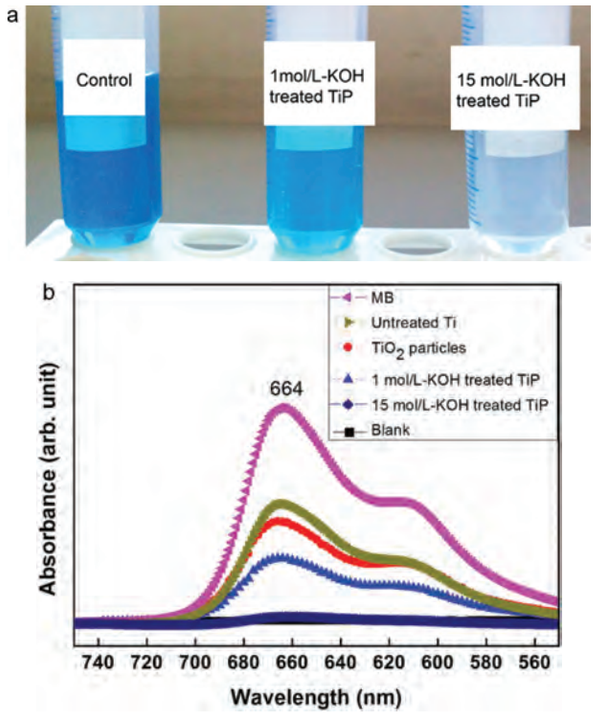

Figure 8. (a) Photographs and (b) UV-Vis absorption spectra taken from the original MB dye, and from the dye exposed to KOH treated Ti particles after UV light irradiation for 2 hours. UV-Vis spectra of untreated Ti particles as well as oxidized Ti particles (TiO_2 particles) are also included for comparison.

3.6.2. Effect of the Surface Charge

Additionally, the effect of surface charge on the photocatalytic activity and the photodegradation of MB dye was studied by varying the pH values (acidic, neutral and alkaline solutions). Figure 9 shows the different decolorization of MB dye after treatment with the 15 mol/L KOH treated Ti particles of different pH, representatively. As can be seen in Figure 9(a), the decolorizing is more significant for pH = 7.0 and 10.0 compared with pH = 2.5. In order to look at this result more into detail, UV-Vis absorption spectra were taken as a function of pH (see Fig. 9(b)). In alkaline environment, the degradation was about 95%, indicating the strong effect of the pH level. In contrast, for pH = 2.5, the degradation was almost not negligible compared with that of the raw MB dye. In order to exclude the formation of the colorless leuco-methylene blue, we

Table I. Values of C/C_0 with different WCP conditions and TiO_2 particles after UV light irradiation for 2 h.

Samples	C/C_0 (after 2 h)
MB	0.98
Untreated	0.87
TiO_2 particles	0.75
1 mol/L KOH treated Ti	0.54
15 mol/L KOH treated Ti	0.09

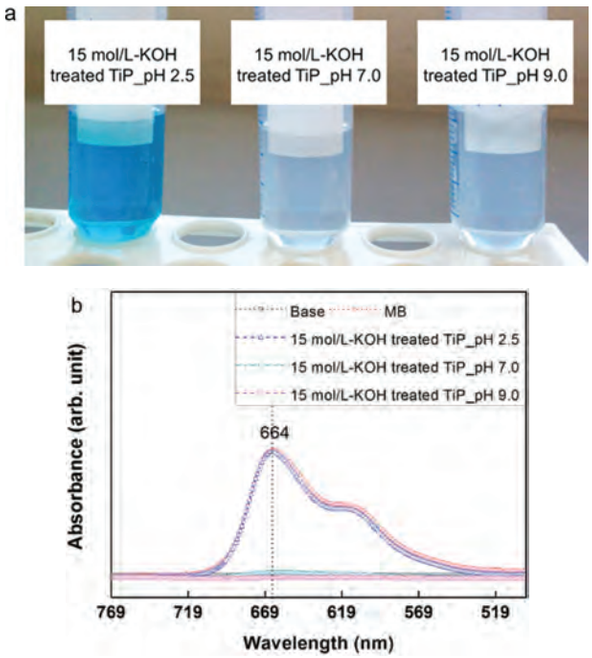

Figure 9. (a) Photographs taken from of MB dye solutions treated with $KTiO_x$ of different surface charge and (b) UV-Vis absorption spectra of MB dye solution and 15 mol/L KOH treated Ti particles at pH 2.5, 7.0, and 9.0 after 2 hours of UV light exposure.

carefully checked the UV-Vis spectra but its characteristic absorption peak at around 310 nm (not shown) couldn't be observed.

Generally, pH is one of the most important parameters for the photocatalytic activity because pH strongly determines the adsorption of molecules onto the catalysts surface.[17] Strong adsorption of the degradable molecules is a prerequisite for the enhancement of the photocatalytic activity. MB dye molecules are known to be cationic. Consequently, negative sites on the surface of catalyst can promote the adsorption of molecules owing to electrostatic interactions. As observed in zeta-potential measurements (Fig. 5), the surface of $KTiO_x$ was charged positively in acidic media below IEP (<pH 4) and negatively charged above IEP (>pH 4). Hence, below IEP, the electrostatic repulsion between MB dye molecules and the positively charged catalyst surface will retard their adsorption and hamper the photocatalytic activity. On the other hand, the strong adsorption between MB dye molecules and negatively charged surface will occur above IEP, resulting in enhanced photocatalytic effect.

The photocatalytic process is based on the generation of electron–hole pairs under UV irradiation, which affects the adsorption–desorption processes and the separation of the photo-generated electron–hole pairs in the surface of the catalyst particles.[17] When a semiconductor absorbs light of energy greater or equal to its band gap, electrons are excited into the conduction band and holes are existed into the valence band. This charge separation induces the formation of electron–hole pairs which can generate free radicals such as hydroxyl (·OH). Active species such as ·OH are very efficient oxidizers of organic dyes, leading to dye fading as shown in Figures 8(a) and 9(a).[42,43] Above IEP, hydroxide ions (OH^-) induce the generation of hydroxyl radicals ·OH, which originate from the photo-induced oxidation of OH^- by holes forming on the $KTiO_x$ surface. Overall, pH strongly affects the adsorption–desorption process and the generation of oxidizer species. Therefore, the degradation efficiency of dyes increases with the pH value owing to the electrostatic interaction between MB dye cations and the negative surface of $KTiO_x$.

3.6.3. *Effect of the Annealing Temperature and Different Dyes*

The photocatalytic degradation of MB, CG and AR dye solutions was studied as a function of the annealing temperature. Figure 10(a) shows the photocatalytic performance of different $KTiO_x$ samples in the MB dye solution. After 2 hours of UV treatment, the $KTiO_x$ annealed at 600 °C showed significantly higher degradation compared with the reference sample of $KTiO_x$ obtained without annealing. The trend is clearly visible: the photocatalytic efficiency increases with the annealing temperature. However, the $KTiO_x$ sample annealed at 750 °C does not follow this trend, and the degradation efficiency drops even below that of pristine $KTiO_x$ reference sample. This can be explained, on the one hand, by the reduced surface area due to the larger diameter of nanowires as well as due to the more entangled nanostructures. On the other hand, annealing at 750 °C promotes the formation of the rutile phase (see Fig. 7), which is known to have a lower density of localized states and to lead to faster charge carrier recombination.[44]

For the CG dye solution, outstanding degradation efficiency, even higher than that of MB dye, was observed, as presented in Figure 10(b). All $KTiO_x$ showed a degradation efficiency higher than 95% under 1 hour UV exposure. The $KTiO_x$ annealed at 450 °C showed the best performance. In the case of AR dye solution, the photocatalytic performance is generally rather low. The KTiOx annealed at 600 °C yielded the highest degradation efficiency of about 32.9%.

3.6.4. *Recovery and Re-Use of $KTiO_x$*

For TiO_2 nanostructures, their separation from aqueous suspension is a major constraint in photocatalytic waste water treatment. The separation is generally energy-intensive as well as cumbersome, and it also does not reach the high recovery efficiency. This aspect remains a serious drawback for potential practical applications.[36]

To analyze the recovery and re-use performance of $KTiO_x$, those particles annealed at 600 °C were studied as their all-round performances in MB, CG, and AR

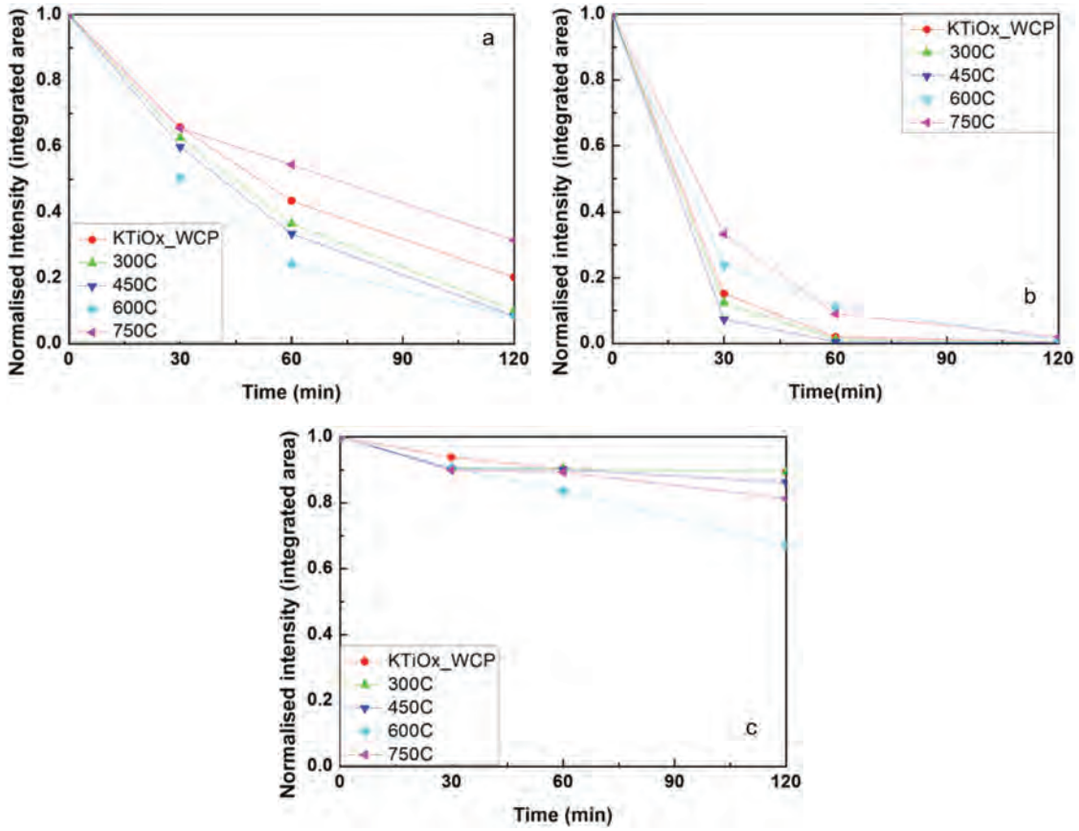

Figure 10. Photocatalytic degradation behaviors of (a) MB dye, (b) CG dye, and (c) AR dye solution treated with $KTiO_x$/Ti particles annealed at different temperatures.

dye solutions were high. The recovered $KTiO_x$ was reused for photocatalysis up to four times. Figure 11 displays the evolution of the degradation efficiency as a function of the number of cycles. In the case of MB dye, the $KTiO_x$ could easily be cleaned by only deionized water and organic solvents (ethanol and isopropanol) without any other additional processes, especially without additional UV treatment for several hours as reported by Kumar et al.[45] The photocatalytic performance remained almost constant up to about 97% after several cycles. Comparable repeatability has been reported for TiO_2 nanotubes fixed on Ti substrate.[46]

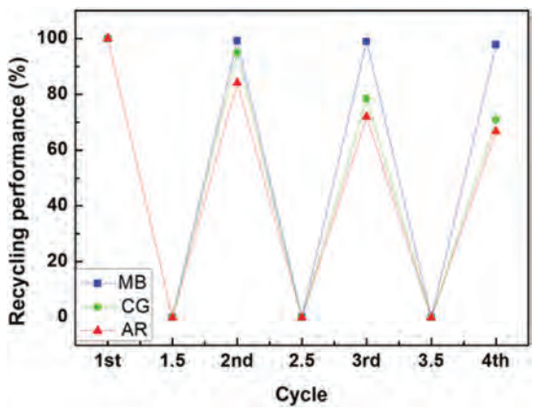

Figure 11. The degradation efficiency variation after UV irradiation cycles in repeated experiments.

The reusability of TiO_2 in CG and AR dye has not been reported much in literature. In our cycled experiments, the photocatalytic performance in the CG dye was reduced to about 71% after 3 cycles. In the AR dye solution, the recycle performance was further weakened to about 67% degradation efficiency in the last cycle, even when additional cleaning via UV irradiation was performed. A possible explanation for this observation is that the organic residues remain attached inside the nanowire network structure and cannot easily be washed out. Why CG and AR dyes are more sensitive to the entrapment is not yet clear and requires more detailed analysis.

It has to be mentioned that the $KTiO_x$ nanostructures produced by the WCP of Ti microspheres enable immobilization of the catalyst directly from the synthesis step. For supported TiO_2, the photochemical reactivity is normally reduced due to the reduction of active surface area and the inactive support hindrance in light harvesting. These implications do not occur for the $KTiO_x$ nanostructures on Ti microspheres. Moreover, the attachment of $KTiO_x$ on Ti is mechanical strong in order to ensure a long term operation.

Together with the simple cleaning procedure (using only water and organic solvents without additional UV irradiation) and the remarkably efficient recycling performance in MB, $KTiO_x$ produced by the WCP has a high potential for re-usable photocatalyst.

4. CONCLUSIONS

We performed a detailed structural and chemical analysis of $KTiO_x$ nanostructures produced by the WCP of Ti microspheres. Their photocatalytic activity was studied as a function of the surface area as well as the surface charge. The $KTiO_x$ nanowires obtained from 15 mol/L KOH solution yielded the highest surface area and also the highest photocatalytic performance. The negatively charged $KTiO_x$ nanostructures which were annealed at 600 °C showed the highest photocatalytic degradation of 92% for MB dye, 99% for CG dye, and 33% for AR dye. This result was attributed to the enhanced active surface area and surface charge as well as the presence of the crystalline layered structure based on the anatase phase. In addition, the $KTiO_x$ nanostructures immobilized on Ti particles offer great advantages for separation from the liquid. Indeed, remarkable recycling performance of 97% for MB dye, 71% for CG dye, and 67% AR dye was obtained after simply washing with deionized water and with organic solvents. We believe that the $KTiO_x$ nanostructures produced by the WCP has a great potential for photocatalysis but also for photovoltaics, bio-and eco-friendly devices, where high catalytic activity and easy cleaning are required.

Acknowledgments: We thank Professor Lutz Mädler for his help and the access to his facilities. This work was supported by the Belgian Hercules Stichting (HER/08/25 and AKUL/13/19) as well as by the Flemish FWO with Odysseus program, the bilateral collaboration project with Korea (VS.039.16N) and FWO research project G0B8915N. We are also grateful to the Research Council of KU Leuven for the project IOF-KP (3E140382).

References and Notes

1. N. Toshima and T. Yonezawa, *New J. Chem.* 22, 1179 (**1998**).
2. R. Narayanan and M. A. El-Sayed, *Nano Lett.* 4, 1343 (**2004**).
3. J. Grunes, J. Zhu, M. Yang, and G. A. Somorjai, *Catal. Lett.* 86, 157 (**2003**).
4. L. E. E. Greene, B. D. D. Yuhas, M. Law, D. Zitoun, and P. Yang, *Inorg. Chem.* 45, 7535 (**2006**).
5. L. G. Devi and R. Kavitha, *Appl. Catal. B Environ.* 140, 559 (**2013**).
6. W. Y. Teoh, J. A. Scott, and R. Amal, *J. Phys. Chem. Lett.* 3, 629 (**2012**).
7. M. N. Chong, B. Jin, C. W. K. Chow, and C. Saint, *Water Res.* 44, 2997 (**2010**).
8. K. Hashimoto, H. Irie, and A. Fujishima, *Jpn. J. Appl. Phys.* 191 (**2005**).
9. Y. Ma, X. L. Wang, Y. S. Jia, X. B. Chen, H. X. Han, and C. Li, *Chem. Rev.* 114, 9987 (**2014**).
10. I. M. Arabatzis and P. Falaras, *Nano Lett.* 3, 2 (**2002**).
11. M. K. Seo and S. J. Park, *J. Nanosci. Nanotechnol.* 11, 4633 (**2011**).
12. H. He, A. Chen, M. Chang, L. Ma, and C. Li, *J. Ind. Eng. Chem.* 19, 1112 (**2013**).
13. L. Chen, Y. Man, and Z. Chen, *Nanotechnology* 25, 165401 (**2014**).
14. S. Y. Chae, M. K. Park, S. K. Lee, T. Y. Kim, S. K. Kim, and W. I. Lee, *Chem. Mater.* 15, 3326 (**2003**).
15. K. Nagaveni, G. Sivalingam, M. S. Hegde, and G. Madras, *Environ. Sci. Technol.* 38, 1600 (**2004**).
16. Z. B. Zhang, C. C. Wang, R. Zakaria, and J. Y. Ying, *J. Phys. Chem. B* 102, 10871 (**1998**).
17. A. Franco, M. C. Neves, M. M. L. R. Carrott, M. H. Mendonça, M. I. Pereira, and O. C. Monteiro, *J. Hazard. Mater.* 161, 545 (**2009**).
18. J. Jaramillo, B. A. Garzón, and L. Tirado Mejía, *J. Phys.: Conf. Ser.* 687, 12099 (**2016**).
19. S. Y. Lee, C. H. Lee, D. Y. Kim, J. Locquet, and J. W. Seo, *Nanomaterials* 5, 1397 (**2015**).
20. L.-C. Chen, C.-M. Huang, and F.-R. Tsai, *J. Mol. Catal. A Chem.* 265, 133 (**2007**).
21. Y. Bessekhouad, D. Robert, J. V. Weber, and N. Chaoui, *J. Photochem. Photobiol. A Chem.* 167, 49 (**2004**).
22. G. Yang, Z. Yan, T. Xiao, and B. Yang, *J. Alloys Compd.* 580, 15 (**2013**).
23. S. Y. Lee, M. Takai, H. M. Kim, and K. Ishihara, *Curr. Appl. Phys.* 9, e266 (**2009**).
24. S. Y. Lee, R. Matsuno, K. Ishihara, and M. Takai, *Appl. Phys. Express* 4, 1 (**2011**).
25. E. Shin, S. Jin, J. Kim, S. J. Chang, B. H. Jun, K. W. Park, and J. Hong, *Appl. Surf. Sci.* 379, 33 (**2016**).
26. E. Shin, S. Jin, and J. Hong, *Appl. Surf. Sci.* 416, 353 (**2017**).
27. S. Y. Lee, R. Matsuno, K. Ishihara, and M. Takai, *Biosens. Bioelectron.* 41, 289 (**2013**).
28. J. Augustynski, *Electrochim. Acta* 38, 43 (**1993**).
29. G. D. Parfitt, *Prog. Surf. Membr. Sci.* 11, 181 (**1976**).
30. T. Yoko, L. Hu, H. Kozuka, and S. Sakka, *Thin Solid Films* 283, 188 (**1996**).
31. A. Di Paola, G. Marcí, L. Palmisano, M. Schiavello, K. Uosaki, S. Ikeda, and B. Ohtani, *J. Phys. Chem. B* 106, 637 (**2002**).
32. K. Tanaka and A. Ozaki, *J. Catal.* 8, 1 (**1967**).
33. M. Misono, E. Ochiai, Y. Saito, and Y. Yoneda, *J. Inorg. Nucl. Chem.* 29, 2685 (**1967**).
34. K. Hashimoto, H. Irie, and A. Fujishima, *Jpn. J. Appl. Phys.* 4, 8269 (**2005**).
35. H. Zhang and J. F. Banfield, *J. Mater. Chem.* 8, 2073 (**1998**).
36. J. Sun, Y. Wang, R. Sun, and S. Dong, *Mater. Chem. Phys.* 115, 303 (**2009**).
37. J. F. Banfield and D. R. Veblen, *Am. Mineral.* 77, 545 (**1992**).
38. Y. Takahashi, N. Kijima, and J. Akimoto, *Chem. Mater.* 18, 748 (**2006**).
39. H. Wang, C. C. Oey, A. B. Djurišiæ, M. H. Xie, Y. H. Leung, K. K. Y. Man, W. K. Chan, A. Pandey, J. M. Nunzi, and P. C. Chui, *Appl. Phys. Lett.* 87 (**2005**).
40. S. Linic, P. Christopher, and D. B. Ingram, *Nat. Mater.* 10, 911 (**2011**).
41. J.-M. Herrmann, H. Tahiri, Y. Ait-Ichou, G. Lassaletta, A. R. González-Elipe, and A. Fernadez, *Appl. Catal. B Environ.* 13, 219 (**1997**).
42. C. L. Torres-Martínez, R. Kho, O. I. Mian, and R. K. Mehra, *J. Colloid Interface Sci.* 240, 525 (**2001**).
43. H. R. Pouretedal, A. Norozi, M. H. Keshavarz, and A. Semnani, *J. Hazard. Mater.* 162, 674 (**2009**).
44. D. A. H. Hanaor and C. C. Sorrell, *J. Mater. Sci.* 46, 855 (**2011**).
45. S. Kumar, D. K. Lodhi, and J. P. Singh, *RSC Adv.* 6, 45120 (**2016**).
46. S. Yuan, L. Yu, L. Shi, J. Wu, J. Fang, and Y. Zhao, *Catal. Commun.* 10, 1188 (**2009**).

Received: 10 October 2017. Accepted: 11 January 2018.